UDK 546.62: 004.942
Original scientific article/Izvirni znanstveni članek

ISSN 1580-2949
Mater. Tehnol.

OPTIMIZATION AND INFLUENCE OF PROCESS PARAMETERS ON ECAD SECTION SHRINKAGE OF 7075 Al ALLOY

VPLIV IN OPTIMIZACIJA PROCESNIH PARAMETROV ECAD NA SKRČEK POSAMEZNIH SEKCIJ ZLITINE VRSTE Al 7075

Jiayun Zhu[1], Tao He[1*], Xilin Chen[1], Xiangyang Du[1], Alexey Vereschaka[2], Jian Li[1], Shanping Deng[1]

[1]School of Mechanical and Automotive Engineering, Shanghai University of Engineering Science, Songjiang 201620, Shanghai, China
[2]Institute of Design and Technological Informatics of the Russian Academy of Sciences, 127994 Moscow, Russia

Prejem rokopisa – received: 2024-11-15; sprejem za objavo – accepted for publication: 2025-03-26

doi:10.17222/mit.2024.1342

The phenomenon of section shrinkage during the equal channel angular drawing (ECAD) process significantly impacts the dimensional precision of a specimen's cross-section, posing a challenge for the industrial implementation of this forming technique. To address this problem, a numerical simulation of the 7075 Al alloy during the ECAD process was conducted using Deform-3D, which revealed the influence of process parameters on ECAD section shrinkage. Through analyzing the results of the orthogonal design, the importance of various process parameters on section shrinkage was researched using range analysis and analysis of variance. A multi-objective optimization approach utilizing a genetic algorithm was developed to determine the optimal process parameter combination, subsequently validated through ECAD experiments. The results demonstrate that shrinkage decreases as the inner and outer angles of the die increase, while it increases with higher friction coefficients and drawing speeds. Among these process parameters, the inner angle is found to have the most significant influence on shrinkage, followed by the friction coefficient and the outer angle, while the drawing speed has the least impact on shrinkage which can be considered negligible. Consequently, the optimal combination of process parameters is identified as an inner angle of 120°, an outer angle of 90°, and a friction coefficient of 0.11.

Keywords: equal channel angular drawing, section shrinkage, orthogonal design, genetic algorithm

Pojav različnega krčenja materiala zaradi vlečenja ali iztiskavanja pod kotom v kanalu enakega preseka (ECAD; angl.: Equal Channel Angular Drawing) je proces, ki močno vpliva na dimenzijsko točnost prečnega preseka izdelkov, ki so izdelani s tem postopkom in tako predstavlja dokaj velik izziv uporaba tega postopka preoblikovanja materialov v industriji. Avtorji v tem članku opisujejo numerično simulacijo aluminijeve zlitine tipa Al7075 med ECAD procesom z uporabo programskega orodja Deform-3D, ki je razkrila vpliv izbranih procesnih parametrov tega procesa na sekcijsko krčenje oziroma krčenje po posameznih izbranih odsekih preoblikovanca. Z analizo rezultatov ortogonalnega dizajna so avtorji ugotavljali vpliv posameznega procesnega parametra na sekcijsko krčenje in njegovo pomembnost s pomočjo območne analize in analizo variance. Z uporabo več-objektnega optimizacijskega pristopa so avtorji razvili genetski algoritem za določitev kombinacije optimalnih procesnih parametrov, ki so ga nato preverili oziroma ovrednotili s praktičnimi ECAD preizkusi. Z rezultati so dokazali, da se krčenje zmanjšuje s povečevanjem notranjega in zunanjega kota (nagiba), medtem ko naraščata koeficient trenja in hitrost vlečenja (deformacije). Med vsemi analiziranimi procesnimi parametri ima notranji kot orodja največji vpliv na skrček. Temu sledita koeficient trenja in zunanji kot orodja, medtem ko je vpliv hitrosti vlečenja najmanjši in ga zato lahko zanemarimo. Posledično so avtorji ugotovili, da so optimalni procesni parametri naslednji: notranji kot orodja 120°, zunanji kot orodja 90° in koeficient trenja 0,11.

Ključne besede: enako kanalsko kotno vlečenje, skrček po posameznih sekcijah, ortogonalni dizajn, genetski algoritem

1 INTRODUCTION

The rapid development of aerospace and aircraft industry has created an urgent demand for high-strength and lightweight Al alloys.[1,2] The 7075 Al alloy has been widely used as a structural material due to its low density, high strength, ductility, toughness and resistance to fatigue.[3–5] In order to meet the manufacturing specifications, it is necessary to modify the alloy composition, incorporate diverse grain-refining additives, or produce refined microstructures through intensive deformation processes, such as forging, accumulative rolling, compressed-torsion and so on. Equal channel angular pressing (ECAP) is recognized as an effective method to enhance the mechanical properties of Al alloys by producing fine-grained microstructures with high densities of dislocations.[6–9] However, as some researchers found that ECAP was not suitable for the continuous processing of long rods, equal channel angular drawing (ECAD) was developed to expand the potential of ECAP for the continuous production of high-strength Al alloys.[10–12]

Zisman et al. proposed that ECAD was proved to be an efficient method to strengthen Al sheets and control their textures due to its high rate of grain refinement and its continuous processability.[13] Pérez et al. found that ECAD could effectively refine the grain size resulting in an increase in the microhardness and tensile strength of the material.[14] While ECAD demonstrates exceptional

*Corresponding author's e-mail:
hetao@sues.edu.cn (Tao He)

Table 1: Chemical composition of 7075-O Al alloy (*w*/%)

Cu	Mg	Zn	Cr	Fe	Mn	Si	Ti	Al
1.2–2.0	2.1–2.9	5.1–6.1	0.18–0.28	0.5	≤0.3	0.4	≤0.2	Bal.

capabilities in grain refinement, material hardness enhancement, and tensile strength improvement, section shrinkage remains a critical barrier to its industrial adoption.[15] Section shrinkage adversely affects a material's dimensional precision and may lead to crack formation and fracture during processing.[16] Current research on the impact of ECAD process parameters on section shrinkage remains unreported, particularly in exploring the strategies to mitigate shrinkage through process parameter optimization.

To address this issue, a systematic investigation about the influence of ECAD process parameters on the section shrinkage of 7075 Al alloy is essential. A key focus of this research is to identify the primary and secondary process parameters affecting ECAD section shrinkage. The orthogonal design is an efficient method that examines each parameter's impact and potential interactions while minimizing the number of experiments.[17–19] For instance, Kim et al. utilized orthogonal design to develop a 50 kg-grade cold-rolled dual-phase (DP) steel and proposed that orthogonal design was an efficient method.[20] Guan et al. employed the orthogonal method to design nine types of Mg-Al-Sn-Mn magnesium alloy and highlighted the practicality of orthogonal design.[21] Chen et al. investigated stress-strain distribution, loads, and maximum principal stress in conventional drawing, optimized the drawing process parameters with the orthogonal experimental method and found it was convenient for statistical analysis.[22] These studies confirm that orthogonal experimental design is a practical, efficient, and convenient tool commonly used for optimizing process parameters.

Moreover, to reduce the section shrinkage rate under the demands of severe plastic deformation, it is essential to identify the optimal combination of process parameters through multi-objective optimization. One of the challenges of multi-objective optimization is the trade-off between improving one performance metric and potentially worsening others.[23–25] To address this, a genetic algorithm is proposed as a solution. Such an algorithm mimics the evolutionary process in biology, adhering to the principle of survival of the fittest, and continuously seeking Pareto optimum solutions within a population.[26–28] Pu et al. demonstrated that the MOGA optimization approach could effectively enhance the thermal performance of ground heat exchangers (GHEs).[29] Sardinas et al. presented a multi-objective optimization technique based on a genetic algorithm and optimized the conflicting objectives of the tool life and operation time, proving that the genetic algorithm was an effective multi-objective optimization method.[30] Li et al. emphasized the versatility and global search capability of a genetic algorithm and combined analysis of variance with the non-dominated sorting genetic algorithm (NSGA-II) to provide a systematic approach for proton exchange membrane fuel cell multi-objective optimization.[31] The application of the genetic algorithm to solve multi-objective optimization problems is thus proven to be a viable strategy.

In light of this, the present study focuses on the 7075 Al alloy, utilizing finite element software to simulate and analyze the ECAD process, and elucidate the influence of process parameters on section shrinkage, thus filling the research gap in this field. The Design-Expert software is employed to conduct an orthogonal design, aiming to identify the primary and secondary process parameters affecting the specimen section shrinkage. In line with the findings, a multi-objective optimization method based on the genetic algorithm is proposed, which can simultaneously optimize the section shrinkage rate and equivalent strain, providing theoretical support for the industrial application of the ECAD process. This optimization aims to achieve optimal process parameters for minimal section shrinkage and provide valuable reference and guidance for establishing ECAD process parameters.

2 MATERIALS AND METHODS

2.1 Material

The chemical composition of the 7075-O Al alloy used in the present study is shown in **Table 1**. To accurately simulate the ECAD forming of 7075-O Al alloy bars, uniaxial drawing experiments were carried out to determine the material's mechanical properties and establish its constitutive model. A drawing specimen with a gauge length of 10 mm, a width of 2 mm, and a thickness of 1.5 mm was designed. Utilizing an Instron-3369 universal testing machine, the drawing tests were performed at strain rates of 0.1 s^{-1}, 1 s^{-1}, and 10 s^{-1}. The Johnson-Cook constitutive model for the material was then constructed using the data obtained with these drawing experiments.

2.2 Finite element simulation experiment

2.2.1 Finite element modeling

Figure 1a illustrates the 3D finite element model for the ECAD process, with the specimen featuring a diameter of 9.6 mm. Given the high hardness of the die material used in the drawing tests, its deformation was deemed negligible. Consequently, the die was modeled as a rigid object, whereas the specimen was treated as a plastic deformable object. The numerical simulations of the ECAD process were conducted using the Deform-3D finite element software, which employed a total of

32,000 mesh elements. The simulations were conducted under a constant temperature of 20 °C. The material's flow stress behavior was governed by the previously established Johnson-Cook constitutive model. To capture the interaction between the specimen and the die, a shear friction model was applied to simulate the frictional effects during the deformation process.

The specimen can be categorically divided into three distinct zones after the deformation: Zone I, Zone II, and Zone III, as illustrated in **Figure 1b**.[32] Zone I is subjected to drawing but is not affected by the die angle, exhibiting minimal section shrinkage, and can be largely disregarded in this context. At the transition from Zone I to Zone II, there is a marked reduction in the cross-sectional area, giving rise to a relatively consistent pattern of section shrinkage of Zone II. Despite being affected by the die angle, Zone III experiences the phenomenon of curling. Hence, the analysis primarily concentrates on these three zones, which are most affected by the shrinkage phenomenon, to elucidate the patterns of the change associated with each process parameter.

2.2.2 Simulation experimental design

In a single-factor experiment, the protocol involves altering only one variable while maintaining all other factors that could affect the outcome at a constant level. To examine the effects of various parameters on the shrinkage rate, a simulation study was performed focusing on four key parameters: the inner angle, the outer angle, the friction coefficient, and the drawing speed. Three levels were selected for each parameter, as detailed in **Table 2**. In addition, an L9 orthogonal array was adopted to conduct nine simulation experiments, with the section shrinkage rate and equivalent strain explicitly defined as the evaluation criteria, systematically assessing the impact of each parameter on the shrinkage rate.

2.2.3 Orthogonal design of the process parameters on ECAD section shrinkage

The orthogonal design method employs a systematic approach to select representative experimental conditions using orthogonal arrays. It organizes experimental plans for testing and employs range analysis and analysis of variance to ascertain the primary and secondary impacts, as well as the significance, of each factor.[33] In this orthogonal design, four parameters were identified as influential factors: the inner angle (A), the outer angle (B), the friction coefficient (C), and the drawing speed (D). The section shrinkage rate and the average equivalent deformation were adopted as evaluation criteria to investigate the pattern of section shrinkage throughout the entire ECAD process. The factors and their respective levels for the simulation experiment are detailed in **Table 3**.

Table 3: Orthogonal design factors and levels

Level	Simulation experiment factors			
	A (°)	B (°)	C	D (mm·s^{-1})
–1	120	30	0.05	5
0	135	60	0.15	25
1	150	90	0.25	45

2.3 ECAD experimental design

To validate the simulation results, two sets of process parameters were chosen for physical ECAD tests. The specimens were subjected to drawing using the hydraulic machine depicted in **Figure 2a**. Subsequently, the specimens were sectioned using a DK7735 EDM wire cutting machine to prepare five cross-sectional samples. The cross-sectional areas of these samples were then imaged using the area measurement test platform shown in **Figure 2b**. The images were quantitatively analyzed with

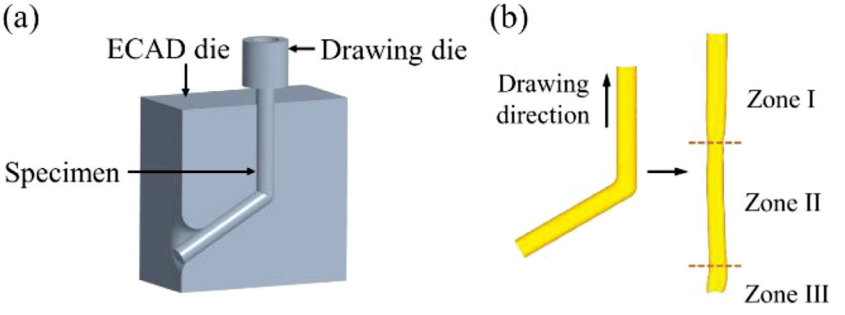

Figure 1: a) 3D schematic diagram of ECAD, b) division of deformation zones of the specimen after ECAD

Table 2: Simulation experimental design

Simulation number	Inner angle (°)	Outer angle (°)	Friction coefficient	Drawing speed (mm·s^{-1})
1	120/135/150	30	0.15	5
2	120	30/60/90	0.15	5
3	120	30	0.05/0.15/0.25	5
4	120	30	0.15	5/25/45

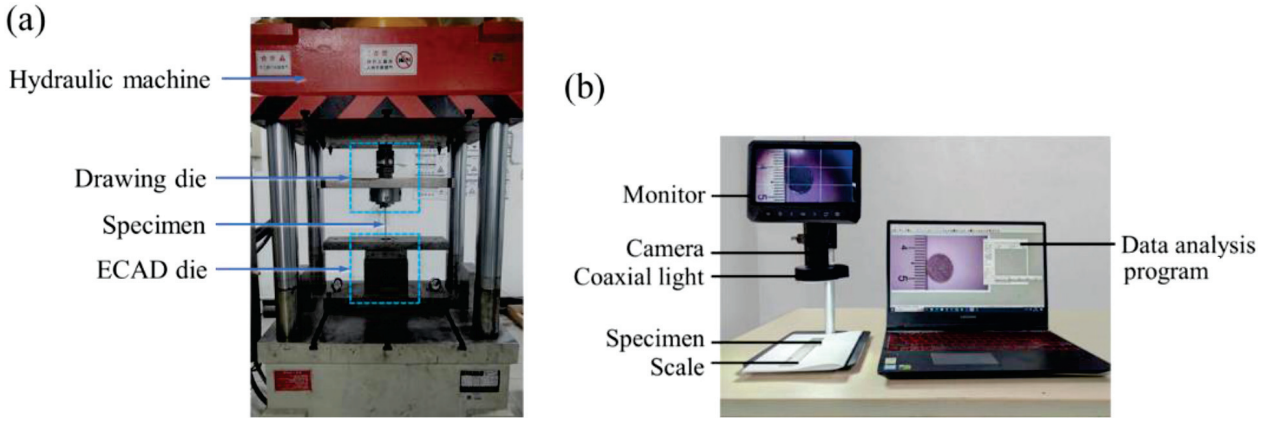

Figure 2: a) Hydraulic machine experimental mold, b) specimen cross-sectional area measurement test platform

the Image-Pro Plus software to determine the average section shrinkage rate accurately.

3 RESULTS AND DISCUSSION

3.1 Establishment of Johnson-Cook constitutive model

The Johnson-Cook constitutive model, introduced in 1983, is an empirical formulation.[34] It posits that the yield stress of a material can be characterized as a function of strain, strain rate and temperature:

$$\sigma = (A + B\varepsilon^{n})\left(1 + C\ln\frac{\dot{\varepsilon}}{\dot{\varepsilon}_0}\right)\left[1 - (T^{*})^{m}\right] \quad (1)$$

Here, $T^{*} = (T - T_r)/(T_m - T_r)$, ε_0 is the reference strain rate, T_m is the melting point of the material, T_r is room temperature, A is the initial yield stress, B is the hardening constant, C is the strain rate constant, m is the thermal softening exponent, and n is the hardening exponent. A higher hardening exponent indicates a more pronounced strain hardening in the material.

The true stress-strain curves for the 7075-O Al alloy, derived from the drawing tests conducted at various strain rates at room temperature, are depicted in **Figure 3**. Through the process of fitting and analyzing the true stress-strain data, the corresponding material coefficients were determined: $T^{*} = 0$, $n = 0.05274$, $A = -291.99677$ MPa, $B = 504.09207$ MPa, $C = 0.0087$. Thus, the expression in the Johnson-Cook constitutive equation can be fitted as follows:

$$\sigma = (-291.99677 + 504.09207\varepsilon^{0.05274})\left(1 + 0.087\ln\frac{\dot{\varepsilon}}{\dot{\varepsilon}_0}\right) \quad (2)$$

Figure 4 illustrates the comparison between the fitted curve derived from the constitutive equation and the actual experimental data points. The close alignment of the curve with the experimental values suggests a robust fit of the constitutive equation, making it an appropriate choice for establishing a material rheological stress database.

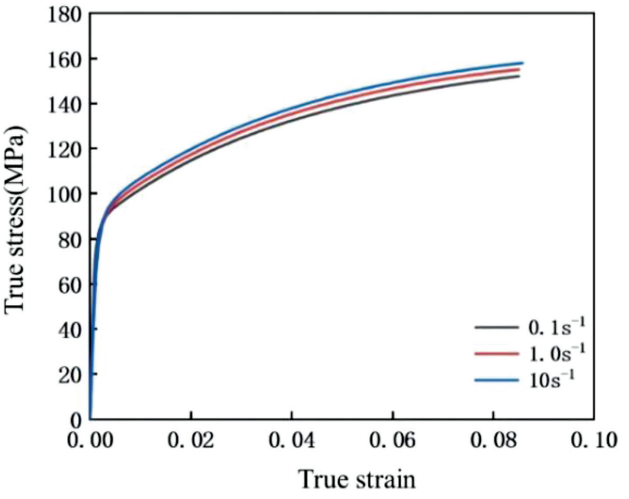

Figure 3: True stress-strain curve of cylinder compression with different strain rates

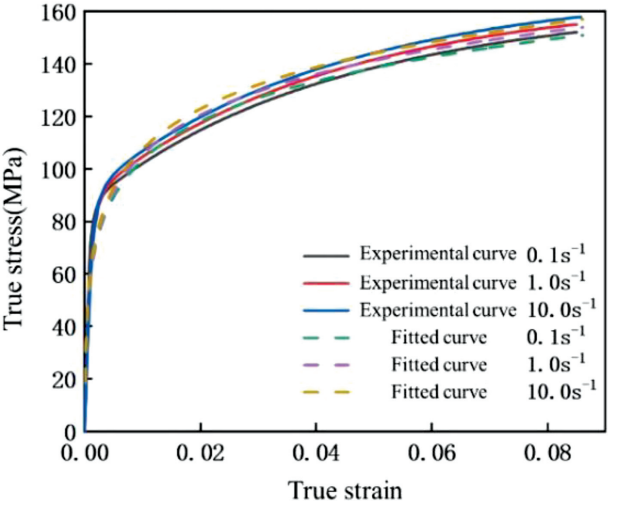

Figure 4: Comparison between the constitutive equation and actual values

3.2 Analysis of the effects of process parameters on ECAD section shrinkage

3.2.1 Effect of inner angle on ECAD section shrinkage

Figure 5 depicts the variation in section shrinkage rates across different zones under varying inner angle conditions. The figure reveals a notable trend: as the inner angle increases, the shrinkage rates at the junctions of Zone I and Zone II, as well as Zone II and Zone III, exhibit a marked decrease. Specifically, these rates decrease from 21 % and 17.6 % at an inner angle of 120° to 10.5 % and 6.8 % at 150°, respectively. Concurrently, the section shrinkage at the boundary between Zone I and Zone II is mitigated, with the smallest diameter of the cross-section increasing from 8.46 mm at 120° to 8.92 mm at 150°, thereby reducing the likelihood of cracking and fracturing.

An increase in the inner angle leads to a reduction in the cumulative equivalent strain, thereby diminishing the shearing effect caused by the inner angle.[35] This reduction in the shearing effect reduces the velocity disparity between the entry and exit points of the die, thus alleviating the section shrinkage phenomenon. Of particular interest is the observation that the section shrinkage rate in Zone II remains relatively stable, while the values of the error bars for the other two Zones are larger. Therefore, the section shrinkage rate of Zone II is chosen as the optimization objective in the subsequent optimization study.

3.2.2 Effect of outer angle on ECAD section shrinkage

Figure 6 illustrates the changes in section shrinkage rates across different zones under varying outer angle conditions. The figure reveals that with the increase in the outer angle, the section shrinkage rate at the junction of Zone I and Zone II experiences a moderate decline. Specifically, there is a decrease from 21 % at an outer angle of 30° to 17.6 % at 90°. Similarly, the section shrinkage rate of Zone II also exhibits a slight reduction, dropping from 17.6 % at 30° to 15.4 % at 90°. Zone III is similar to the previous values.

A larger outer angle reduces the shearing effect on the specimen, thereby decreasing the equivalent strain. However, the increase in the outer angle enhances the positive pressure between the specimen and the inner wall of the die corner. This heightened pressure results in an augmented frictional force and a more pronounced speed differential between the specimen's entry and exit points. These factors contribute to insufficient metal flow and a slight decline in the section shrinkage rate. It is important to note that the outer angle exerts a relatively minor influence on the section shrinkage of the specimen compared to the inner angle.

3.2.3 Effect of drawing speed on ECAD section shrinkage

Figure 7 displays a specific trend in section shrinkage rates across various zones at different drawing speeds. It is evident from the data that an increase in the drawing speed corresponds to a moderate rise in the section shrinkage rates at the junctions of Zone I and Zone II, as well as Zone II and Zone III, although the rate of increase is relatively slow. The 7075-O Al alloy's strain rate sensitivity, as indicated by its constitutive equation, is quite low, with a coefficient of 0.0087. This suggests that the material's response to the changes in drawing speed should be limited. Nonetheless, the thermodynamic perspective offers a contrasting view. Over 90 % of the work input into the specimen is converted into heat, while only a minor portion contributes to the deformation process. This heat is not easily dissipated from the die, leading to a localized temperature increase in the specimen. As the drawing speed is incremented, the rate at which work is converted into heat intensifies, resulting in a more pronounced temperature rise within the speci-

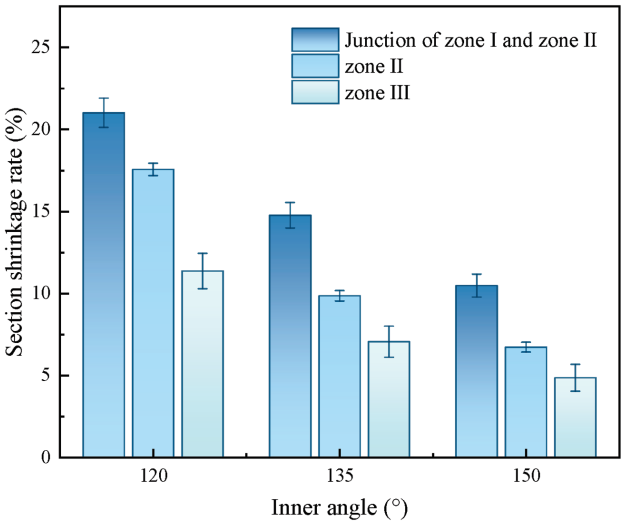

Figure 5: Variation in the section shrinkage rate in different areas at different inner angles

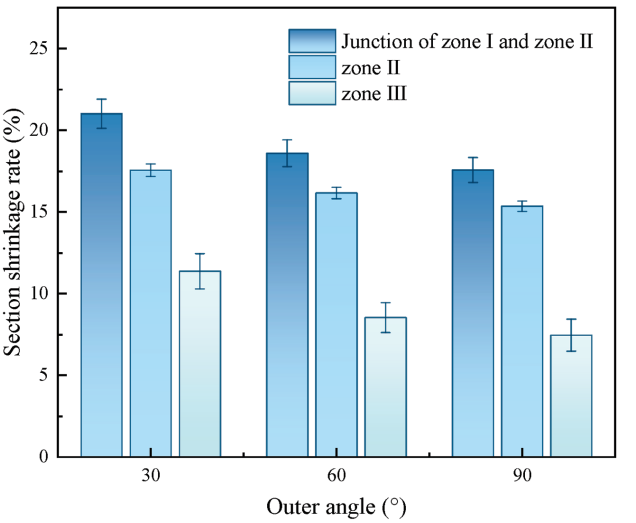

Figure 6: Variation in the section shrinkage rate in different areas at different outer angles

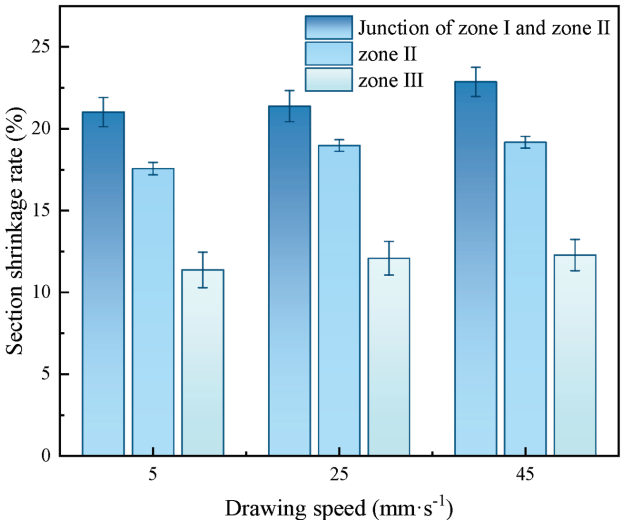

Figure 7: Variation in the section shrinkage rate in different areas at different drawing speeds

men. This thermal effect is accompanied by a reduction in the material's yield strength and an increase in its deformability, which in turn leads to the observed increase in section shrinkage rates.

3.2.4 Effect of friction coefficient on ECAD section shrinkage

Figure 8 provides insights into the impact of varying friction coefficient on the section shrinkage rates of different zones. The data clearly indicates that as the friction coefficient increases, there is a marked escalation in the section shrinkage rate at the junction of Zone I and Zone II, which increases from 18.6 % at a friction coefficient of 0.05 to 22.3 % at 0.25. The section shrinkage rates of Zone II and Zone III also experience an upward trend with the rising friction coefficient, though at a more gradual pace.

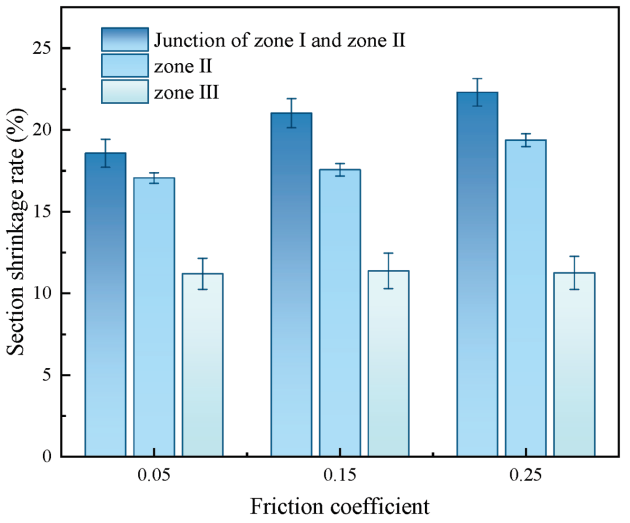

Figure 8: Variation in the section shrinkage rate in different areas at different friction coefficients

Previous research established that an increase in the friction coefficient leads to a direct proportional increase in the frictional force between the specimen and the inner wall of the die corner. This results in a higher frictional force per unit area, which in turn enhances yielding and aggravates section shrinkage, leading to an escalation in the section shrinkage rate. The pronounced section shrinkage at the boundary between Zones I and II causes the specimens to partially detach from the inner wall of the die corner, thereby reducing the shearing effect. As a consequence, even with a higher friction coefficient, the section shrinkage rate in Zone II increases at a slower rate.

3.3 Optimization of process parameters

3.3.1 Orthogonal design

Considering the stringent precision demands of the experimental protocol, the economic considerations related to resource allocation, and the complex interplay among the various factors, the research team chose to employ a 4-factor, 3-level orthogonal array design for the study. This approach optimizes the number of experimental runs needed to investigate the influences of multiple factors simultaneously. The experimental configurations of this research were generated through simulations conducted with the Deform-3D software. For the quantification of cross-sectional areas, we relied on Image-Pro Plus software, which provided precise measurements necessary for the analysis. Using these measurements, the section shrinkage rates for each set of specimens were computed. The findings from the orthogonal design are detailed in **Table 4**, offering a comprehensive overview of the outcomes, and facilitating the interpretation of the effects of the various factors on section shrinkage rates.

Table 4: Orthogonal design results

Test number	A (°)	B (°)	C	D (mm·s^{-1})	Section shrinkage rate (%)	Equivalent strain
1	120	30	0.05	5	15.6	0.502
2	120	60	0.15	25	16.7	0.513
3	120	90	0.25	45	18.3	0.543
4	135	30	0.15	45	13.6	0.393
5	135	60	0.25	5	15.7	0.431
6	135	90	0.05	25	13.3	0.402
7	150	30	0.25	25	10.2	0.275
8	150	60	0.05	45	8.9	0.271
9	150	90	0.15	5	8.3	0.273

3.3.2 Range analysis and analysis of variance

The intuitive analysis of the orthogonal design is based on a thorough comparison of results, aiming to ascertain the influence of different levels of each factor on the experimental outcomes by examining the range of values. This range serves as an indicator of the relative importance of each factor; a broader range signifies a

more substantial impact on the experimental indices, thus marking the factor as more critical.[36] **Table 5** presents the intuitive analysis pertaining to the section shrinkage rate derived from the simulation experimental data. The analysis reveals the hierarchy of influence exerted by the four considered factors on the section shrinkage rates, ranking them as follows: the inner angle (Factor A) exerting the most significant influence, followed by the friction coefficient (Factor C), the outer angle (Factor B), and the drawing speed (Factor D) having the least effect.

Table 5: Range analysis results for the section shrinkage rate

Factor	A (°)	B (°)	C	D (mm·s^{-1})
$\overline{K}_1$	16.867	13.133	12.6	13.2
$\overline{K}_2$	14.2	13.767	12.867	13.4
$\overline{K}_3$	9.133	13.3	14.733	13.6
Range	7.734	0.634	2.133	0.4

Table 6 intuitively shows the ranking of the range of influences on equivalent strain from the four factors: inner angle (A) > friction coefficient (C) > drawing speed (D) > outer angle (B). Hence, it can be inferred that the inner angle has the greatest impact on the equivalent strain, followed by the friction coefficient and drawing speed, whereas the outer angle has the smallest impact on the equivalent strain.

Table 6: Range analysis results for the equivalent strain

Factor	A (°)	B (°)	C	D (mm·s^{-1})
$\overline{K}_1$	0.519	0.390	0.271	0.402
$\overline{K}_2$	0.288	0.405	0.393	0.276
$\overline{K}_3$	0.273	0.285	0.416	0.402
Range	0.246	0.12	0.145	0.126

These rankings demonstrate that the inner angle is the most critical factor influencing the section shrinkage rates. This phenomenon can be explained with the material flow behavior: a large inner angle reduces the accumulation of the shear strain at the die corner.[35] When the inner angle increases, the material's flow path becomes smoother, reducing the velocity gradient and thereby alleviating the shrinkage phenomenon caused by uneven local plastic deformation. Additionally, a small shear strain also decreases the dislocation density, reducing the tendency of material hardening and further suppressing the section shrinkage. The friction coefficient also plays a crucial role, indicating that the interaction between the specimen and the die surface is a key consideration. A high friction coefficient enhances the constraint of the die inner wall on the material, hindering the metal flow and generating a greater normal pressure at the corner. This constraint leads to localized severe deformation of the material, thereby exacerbating the section shrinkage.

The outer angle's influence is less pronounced than those of the inner angle and friction coefficient, but still notable. This is probably due to an increase in the outer angle, which slightly raises the normal pressure of the die on the material, promoting the filling of the material at the corner and thereby compensating for the shrinkage caused by the flow lag. However, this effect is limited by the weak ability of the outer angle to regulate the overall strain distribution, resulting in its relatively low influence. Finally, the drawing speed appears to have the least impact on the section shrinkage rates among the factors studied, suggesting that changes in this parameter result in relatively minor fluctuations in the shrinkage outcomes. This is because the temperature increase is limited and insufficient to significantly alter the yield behavior of the material within the experimental speed range.

The range analysis, while providing a preliminary understanding of the factors' influence on the experimental outcomes, indeed falls short in accounting for the impact of experimental errors on the results. To validate the findings from the range analysis and to gain a more nuanced understanding of the statistical significance of each factor, the analysis of variance is essential. This statistical method assesses the significance of the orthogonal design by comparing the P-values associated with each factor. The P-value is a critical metric in the analysis of variance, serving as an indicator of a factor's statistical significance. A P-value greater than 0.05 suggests that the factor's effect is not statistically significant, meaning that the observed differences could be due to random variation. Conversely, a P-value lower than 0.05 indicates that the factor's effect is statistically significant, implying that the differences observed are unlikely to be due to chance alone.[37] In the context of this study, the minimal impact of the drawing speed on section shrinkage rates led to its designation as a residual error term in the analysis of variance. This decision reflects the understanding that its influence on the experimental outcomes is insufficient to warrant independent consideration as a significant factor.

As shown in **Table 7**, the analysis of variance indicates that both the inner angle (Factor A) and the friction coefficient (Factor C) exert statistically significant effects on section shrinkage rates. This is evidenced by their respective P-values of $P_A = 0.0026$ and $P_C = 0.028$, both of which are below the 0.05 threshold. This confirms the importance of these factors in influencing the experimental results. For the outer angle (Factor B), the P-value is $P_B = 0.2707$, which is greater than 0.05. This indicates that the outer angle does not have a statistically

Table 7: Analysis of variance results for section shrinkage rates

Source of error	Sum of squares	Degree of freedom	Mean square	F-value	P-value
A	92.59	2	46.29	385.78	0.0026
B	0.6467	2	0.3233	2.69	0.2707
C	8.11	2	4.05	33.78	0.0288
Residual error	0.24	2	0.07	–	–
Total	101.58	8	–	–	–

significant effect on section shrinkage, aligning with the range analysis results that ranked its influence as relatively low. The consistency between the analysis of variance and the range analysis reinforces the conclusion that the outer angle is a less critical factor in the context of section shrinkage rates.

The variance results presented in **Table 8** reveal that the P-values for the inner angle (Factor A) and the friction coefficient (Factor C) are P_A = 0.0007 and P_C = 0.0499, respectively, both of which are below the 0.05 threshold. This indicates that both the inner angle and the friction coefficient have a significant influence on the equivalent strain. In contrast, the outer angle (Factor B) has a P-value of P_B = 0.1118, which is above 0.05, implying that it has a relatively minor impact on the equivalent strain. This finding is consistent with the range analysis, which also indicated a lower influence of the outer angle on the equivalent strain compared to the other factors.

Table 8: Analysis of variance results for the equivalent strain

Source of error	Sum of squares	Degree of freedom	Mean square	F-value	P-value
A	0.0913	2	0.0457	1505.48	0.0007
B	0.0005	2	0.0002	7.95	0.1118
C	0.0012	2	0.0006	19.03	0.0499
Residual error	0.0001	2	0	–	–
Total	0.093	8	–	–	–

3.3.3 Analysis of ECAD verification experiment

The thorough analysis of individual factors affecting the section shrinkage, coupled with the orthogonal significance analysis of process parameters, elucidated that the inner angle, friction coefficient, and outer angle all exert significant influence on both the section shrinkage and equivalent strain. To quantify the relationship between these three factors and the outcomes of interest, a multivariate linear regression analysis was performed using the Minitab software. This analysis resulted in an R-squared value of 0.9507 and an adjusted R-squared value of 0.9212 for section shrinkage, signifying a robust model fit. The regression equation can be presented as follows:

$$Y_1 = 46.43 - 0.2578A + 0.0028B + 10.67C \quad (3)$$

The regression analysis for equivalent strain yielded an R-squared value of 0.9923 and an adjusted R-squared value of 0.9877, signifying an excellent fit of the model. The regression equation representing this relationship is as follows:

$$Y_2 = 1.4743 - 0.008211A + 0.000267B + 0.1233C \quad (4)$$

To corroborate the precision of the model, experimental validation is performed by aligning theoretical model calculations with empirical data. Two sets of process parameters are chosen for the ECAD tests. The corresponding experimental images are depicted in **Figure 9**.

The reconciliation of experimental outcomes and theoretical model predictions is documented in **Table 9**. As can be seen from the table, the simulation results exhibit a high degree of consistency with the experimental data. Under the conditions of an inner angle of 120°, outer angle of 30°, friction coefficient of 0.05, and drawing speed of 5 mm/s, the simulated section shrinkage rate was 15.58 %, while the experimentally measured value was 14.73 %, resulting in a relative error of 5.48 %. Similarly, under the conditions of an inner angle of 135°, outer angle of 30°, friction coefficient of 0.05, and drawing speed of 5 mm/s, the relative error was 2.42 %. These results indicate that the finite element simulation can effectively predict the section shrinkage during the ECAD process.

Table 9: Theoretical and experimental results for the section shrinkage

Number	A (°)	B (°)	C	D (mm·s^{-1})	Theoretical value (%)	Experimental value (%)	Relative error (%)
1	120	30	0.05	5	15.58	14.73	5.48
2	135	30	0.05	5	12.24	12.54	2.42

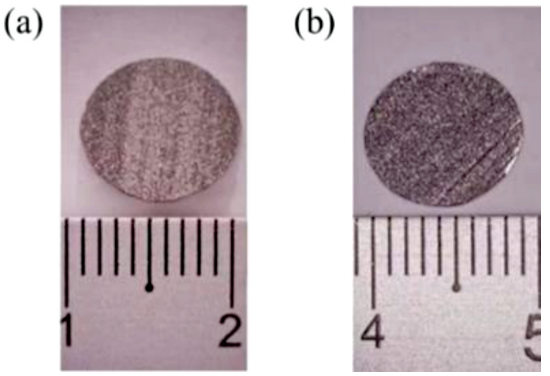

Figure 9: Experimental results: a) inner angle of 120° and outer angle of 30°; b) inner angle of 135° and outer angle of 30°

3.3.4 Multi-objective optimization through NSGA-II

To attain the smallest section shrinkage rate for the specimen following the ECAD process, while simultaneously ensuring the material's mechanical performance equivalent strain requirements are met, a multi-objective optimization model is formulated using the target functions Y_1 and Y_2 derived from the multivariate linear regression analysis. Additionally, the model's constraint conditions must be defined. Specifically, the inner angle must be greater than 120° to prevent excessive deformation that could lead to specimen fracture, and it must be less than 150° to ensure sufficient deformation for the desired effect. Similarly, the outer angle of the die is constrained between 30° and 90° to balance forming effectiveness and deformation. Furthermore, the selection

of the friction coefficient encompasses values with and without lubrication, as shown below:

$$F_{\min} = [Y_{1'} - Y_2]$$
$$st. \begin{cases} 120 \le A \le 150 \\ 30 \le B \le 90 \\ 0.05 \le C \le 0.25 \end{cases} \quad (5)$$

The objective functions and constraints were integrated into the MATLAB NSGA-II genetic algorithm, which was set with a population size of 600, 200 iterations, a crossover probability of 0.9, and a mutation probability of 1/3. The resulting Pareto frontier plot is depicted in **Figure 10**, providing a visual representation of the trade-offs between the objectives.

The Pareto front obtained from the NSGA-II genetic algorithm reveals a positive correlation between the section shrinkage rate and the equivalent strain. In region A, the equivalent strain exhibits a linear increase with the section shrinkage rate, indicating substantial variability. In region B, a turning point is observed when the increase in the section shrinkage rate leads to a flattening trend in the equivalent strain. In region C, the equivalent strain shows minimal change with an increasing section shrinkage rate. It is advisable to select the parameters within region B, as it ensures that both the section shrinkage rate and equivalent strain remain within the acceptable ranges while optimizing both objectives. Consequently, selecting a solution from region B yields a satisfactory multi-objective optimization result, with the process parameters rounded to an inner angle of 120°, an outer angle of 90°, and a friction coefficient of 0.11. These optimized variables and results are presented in **Table 10**.

Table 10: Multi-objective optimization Pareto solution

Optimization variables		Optimization results		
Inner angle (°)	Outer angle (°)	Friction coefficient	Section shrinkage rate (%)	Equivalent strain
120	90	0.11	16.62	0.5255

ri0To validate the precision of the multi-objective optimization outcomes, the specified process parameters were employed in an ECAD test conducted at a drawing speed of 5 mm·s^{-1}. The experimental results yielded a section shrinkage rate of 14.97 %. When compared to the optimized value of 16.62 %, the relative error is 9.93 %. These results validate the accuracy and reliability of the multi-objective optimization model.

4 CONCLUSIONS

(1) In this study, the impact of ECAD process parameters on the section shrinkage of a specimen is elucidated through ECAD simulation experiments. The section shrinkage rate is found to decrease with an increase in both the inner and outer angles of the die. Conversely, it increases with a higher friction coefficient and drawing speed.

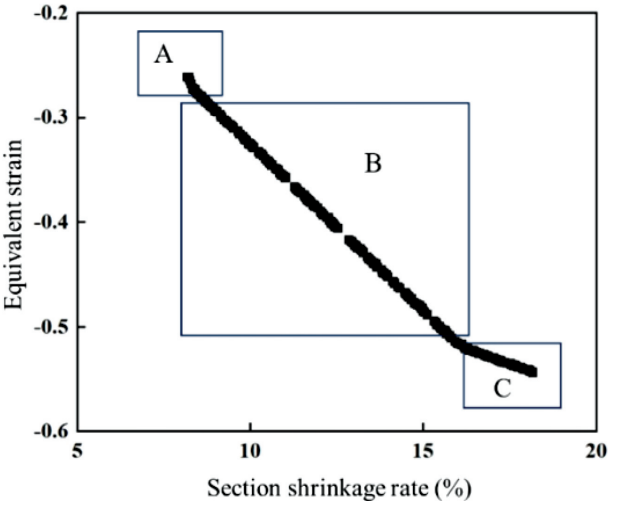

Figure 10: Multi-objective Pareto optimization results

(2) By conducting the analysis of variance and the range analysis on the results of orthogonal design, the primary and secondary factors of the four process parameters are ascertained. Among the studied parameters, the inner angle exerts the most significant influence on shrinkage, followed by the friction coefficient and the outer angle, while the drawing speed has the least impact.

(3) By employing a multi-objective genetic algorithm, the Pareto optimum solution that balances equivalent strain and sectional shrinkage rate is determined. The optimal combination of process parameters includes an inner angle of 120°, an outer angle of 90°, and a friction coefficient of 0.11, while the accuracy of these optimized results is confirmed by the ECAD experiment.

The optimized process parameters substantially mitigate the section shrinkage, enhancing the dimensional accuracy of high-strength aluminum alloy components. Furthermore, this study offers theoretical and practical insights required for an industrial application of the ECAD process. The proposed optimization methods and experimental framework are also applicable to other materials, highlighting their broad potential.

Acknowledgements

This work was supported by the National Natural Science Foundation of China (Grant No.52275350) and International Cooperative Scientific Research Platform of SUES (Grant No.0301006).

Contributions

Jiayun ZHU (ORCID: 0009-0005-5698-0380): data curation, methodology, investigation, writing the original draft. Tao HE: funding acquisition, supervision, project

administration, writing a review & editing. Xilin CHEN: data curation, methodology, investigation, writing a review & editing. Xiangyang DU: writing a review & editing. Alexey Vereschaka: writing a review & editing. Jian LI: writing a review & editing. Shanping DENG: writing a review & editing.

Competing interests

All contributing authors hereby affirm that they have no conflicts of interest pertaining to this study. We reiterate our unequivocal declaration that there are no conflicts of interest associated with the submitted work, including any commercial or ancillary interests.

6 REFERENCES

[1] G. Li, H. Lu, X. Hu, F. Lin, X. Li, Q. Zhu, Current progress in rheoforming of wrought aluminum alloys: A review, Metals, 10 (**2020**) 2, 238, doi:10.3390/met10020238

[2] J. Gao, T. He, Y. Huo, M. Song, T. Yao, W. Yang, Comparison of modified Mohr–Coulomb model and Bai–Wierzbicki model for constructing 3D ductile fracture envelope of AA6063, Chinese Journal of Mechanical Engineering, 34 (**2021**), 1–13, doi:10.1186/s10033-021-00549-4

[3] J. Li, T. He, X. Du, A. Vereschaka, Enhancing the corrosion resistance of high-strength Al-Zn-Mg-Cu alloys after equal channel angular pressing by developing retrogression and re-aging strategies, Corrosion Science, 246 (**2025**), 112736, doi:10.1016/j.corsci.2025.112736

[4] M. Tajally, E. Emadoddin, Mechanical and anisotropic behaviors of 7075 aluminum alloy sheets, Materials & Design, 32 (**2011**) 3, 1594–1599, doi:10.1016/j.matdes.2010.09.001

[5] D. Jia, T. He, M. Song, Y. Huo, X. Du, A. Vereshchaka, J. Li, H. Hu, Microstructure evolution of 7050 Al alloy fasteners during cold upsetting after equal channel angular pressing, Journal of Central South University, 30 (**2023**) 11, 3682–3695, doi:10.1007/s11771-023-5464-8

[6] R. Z. Valiev, T. G. Langdon, Principles of equal-channel angular pressing as a processing tool for grain refinement, Progress in Materials Science, 51 (**2006**) 7, 881–981, doi:10.1016/j.pmatsci.2006.02.003

[7] D. Jia, T. He, M. Song, Y. Huo, H. Hu, Effects of equal channel angular pressing and further cold upsetting process on the kinetics of precipitation during aging of 7050 aluminum alloy, Journal of Materials Research and Technology, 26 (**2023**), 5126–5140, doi:10.1016/j.jmrt.2023.08.258

[8] J. Li, T. He, X. Du, A. Vereschaka, J. Zhang, Regulating hardness homogeneity and corrosion resistance of Al-Zn-Mg-Cu alloy via ECAP combined with inter-pass aging, Materials Characterization, (**2024**), 114489, doi:10.1016/j.matchar.2024.114489

[9] J. Zhang, T. He, X. Du, Y. Huo, D. Jia, X. Chen, Effect of Pre-Equal Channel Angular Pressing Homogenization on Microstructure and Mechanical Properties of As-Cast 7050 Al Alloy, Journal of Materials Engineering and Performance, (**2024**), 1059–9495, doi:10.1007/s11665-024-09950-1

[10] U. Chakkingal, A. B. Suriadi, P. F. Thomson, Microstructure development during equal channel angular drawing of Al at room temperature, Scripta Materialia, 39 (**1998**) 6, 677–684, doi:10.1016/S1359-6462(98)00234-6

[11] U. Chakkingal, A. B. Suriadi, P. F. Thomson, The development of microstructure and the influence of processing route during equal channel angular drawing of pure aluminum, Materials Science and Engineering: A, 266 (**1999**) 1–2, 241–249, doi:10.1016/S0921-5093(98)01129-0

[12] J. León, C. J. Luis-Pérez, Analysis of stress and strain in the equal channel angular drawing process, Materials Science Forum, 526 (**2006**), 19–24, doi:10.4028/www.scientific.net/MSF.526.19

[13] A. A. Zisman, V. V. Rybin, S. Boxel, M. Seefeldt, B. Verlinden, Equal channel angular drawing of aluminium sheet, Materials Science and Engineering: A, 427 (**2006**) 1–2, 123–129, doi:10.1016/j.msea.2006.04.007

[14] C. J. L. Pérez, C. Berlanga, J. Pérez-Ilzarbe, Processing of aluminium alloys by equal channel angular drawing at room temperature, Journal of Materials Processing Technology, 143–144 (**2003**), 105–111, doi:10.1016/S0924-0136(03)00329-7

[15] J. Alkorta, M. Rombouts, J. Messemaeker, L. Froyen, J. G. Sevillano, On the impossibility of multi-pass equal-channel angular drawing, Scripta Materialia, 47 (**2002**) 1, 13–18, doi:10.1016/S1359-6462(02)00089-1

[16] L. Zichao, S. Bin, S. Fanghong, Z. Zhiming, G. Songshou, Diamond-coated tube drawing die optimization using finite element model simulation and response surface methodology, Proceedings of the Institution of Mechanical Engineers Part B: Journal of Engineering Manufacture, 228 (**2014**) 11, 1432–1441, doi:10.1177/0954405413518513

[17] Z. Feng, W. Niu, C. Cheng, S. Liao, Hydropower system operation optimization by discrete differential dynamic programming based on orthogonal experiment design, Energy, 126 (**2017**), 720–732, doi:10.1016/j.energy.2017.03.069

[18] E. Jiaqiang, D. Han, A. Qiu, H. Zhu, Y. Deng, J. Chen, X. Zhao, W. Zuo, H. Wang, J. Chen, Q. Peng, Orthogonal experimental design of liquid-cooling structure on the cooling effect of a liquid-cooled battery thermal management system, Applied Thermal Engineering, 132 (**2018**), 508–520, doi:10.1016/j.applthermaleng.2017.12.115

[19] S. Chen, X. Hong, C. J. Harris, Sparse kernel regression modeling using combined locally regularized orthogonal least squares and D-optimality experimental design, IEEE Transactions on Automatic Control, 48 (**2003**) 6, 1029–1036, doi:10.1109/TAC.2003.812790

[20] S. J. Kim, Y. G. Cho, C. S. Oh, D. E. Kim, M. B. Moon, H. N. Han, Development of a dual phase steel using orthogonal design method, Materials & Design, 30 (**2009**) 4, 1251–1257, doi:10.1016/j.matdes.2008.06.017

[21] M. Guan, Y. Hu, T. Zheng, T. Zhao, F. Pan, Composition optimization and mechanical properties of Mg-Al-Sn-Mn alloys by orthogonal design, Materials, 11 (**2018**) 8, 1424, doi:10.3390/ma11081424

[22] D. C. Chen, J. Y. Huang, Design of brass alloy drawing process using Taguchi method, Materials Science and Engineering: A, 464 (**2007**) 1–2, 135–140, doi:10.1016/j.msea.2007.01.139

[23] G. R. Harik, F. G. Lobo, D. E. Goldberg, The compact genetic algorithm, IEEE transactions on evolutionary computation, 3 (**1999**) 4, 287–297, doi:10.1109/4235.797971

[24] K. M. Hamdia, X. Zhuang, T. Rabczuk, An efficient optimization approach for designing machine learning models based on genetic algorithm, Neural Computing and Applications, 33 (**2021**) 6, 1923–1933, doi:10.1007/s00521-020-05035-x

[25] H. Kumar, R. Manna, D. Khan, Evaluation of Johnson–Cook material model parameters for Fe–30Mn–9Al–0.8C low-density steel in metal forming applications, Journal of Materials Science, 58 (**2023**) 19, 8118–8129, doi:10.1007/s10853-023-08485-5

[26] R. Saravanan, P. Asokan, M. Sachidanandam, A multi-objective genetic algorithm (GA) approach for optimization of surface grinding operations, International Journal of Machine Tools and Manufacture, 42 (**2002**) 12, 1327–1334, doi:10.1016/S0890-6955(02)00074-3

[27] Z. Z. Wang, A. Sobey, A comparative review between Genetic Algorithm use in composite optimisation and the state-of-the-art in evolutionary computation, Composite Structures, 233 (**2020**), 111739, doi:10.1016/j.compstruct.2019.111739

[28] S. Dehuri, R. Mall, Predictive and comprehensible rule discovery using a multi-objective genetic algorithm, Knowledge-Based Systems, 19 (**2006**) 6, 413–421, doi:10.1016/j.knosys.2006.03.004

[29] L. Pu, D. Qi, L. Xu, Y. Li, Optimization on the performance of ground heat exchangers for GSHP using Kriging model based on MOGA, Applied Thermal Engineering, 118 (**2017**), 480–489, doi:10.1016/j.applthermaleng.2017.02.114

[30] R. Q. Sardinas, M. R. Santana, E. A. Brindis, Genetic algorithm-based multi-objective optimization of cutting parameters in turning processes, Engineering Applications of Artificial Intelligence, 19 (**2006**) 2, 127–133, doi:10.1016/j.engappai.2005.06.007

[31] H. Li, B. Xu, G. Lu, C. Du, N. Huang, Multi-objective optimization of PEM fuel cell by coupled significant variables recognition, surrogate models and a multi-objective genetic algorithm, Energy Conversion and Management, 236 (**2021**), 114063, doi:10.1016/j.enconman.2021.114063

[32] X. Chen, T. He, Y. Huo, X. Du, J. Zhang, J. Li, C. Zhang, Simulation and experiment on equal channel angular drawing for 7075 aluminum alloy at room temperature, Forging & Stamping Technology, 48 (**2023**) 11, 67–72, doi:10.13330/j.issn.1000-3940.2023.11.011

[33] M. Ge, C. Du, Preparation process of shear thickening gel based on constrained uniform mixture design and orthogonal experimental design, Polymer Testing, 129 (**2023**), 108267, doi:10.1016/j.polymertesting.2023.108267

[34] A. Shrot, M. Bäker, Determination of Johnson–Cook parameters from machining simulations, Computational Materials Science, 52 (**2012**) 1, 298–304, doi:10.1016/j.commatsci.2011.07.035

[35] Y. Iwahashi, Z. Horita, M. Nemoto, J. Wang, T. G. Langdon, Principle of equal-channel angular pressing for the processing of ultra-fine grained materials, Scripta Materialia, 35 (**1996**) 2, 143–146, doi:10.1016/1359-6462(96)00107-8

[36] Y. Yang, L. Zhou, H. Zhou, W. Lv, J. Wang, W. Shi, Z. He, Optimal design of slit impeller for low specific speed centrifugal pump based on orthogonal test, Journal of Marine Science and Engineering, 9 (**2021**) 2, 121, doi:10.3390/jmse9020121

[37] S. R. Shuken, M. W. McNerney, Costs and benefits of popular P-value correction methods in three models of quantitative omic experiments, Analytical Chemistry, 95 (**2023**) 5, 2732–2740, doi:10.1021/acs.analchem.2c03719